Constructing low-dimensional molecular networks on metal surfaces

Pham, Tuan Anh

Chapter 5

Self-assembly of pyrene derivatives on Au(111): substituent effects on intermolecular interactions*

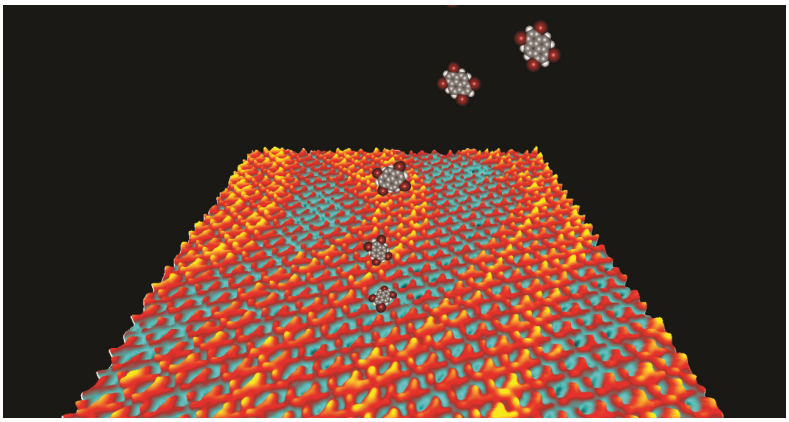

Halogen bonding is recently expected to open up new opportunities for the construction of molecular networks on metal surfaces for future applications. However, the exact role of the halogen substituents in the structural formation of such networks is less studied and thus, asks for more studies in order to efficiently employ halogen bonding for the controlled construction of on-surface assemblies. This has triggered our interest to investigate the influence of halogen substituents on the resulting intermolecular interactions of halogenated molecules on metal surfaces. In this chapter, we investigated the self-assembly of two bromine-functionalized pyrene derivatives on Au(111) by a combination of scanning tunneling microscopy, low energy electron diffraction under ultrahigh vacuum conditions and density functional theory calculations. We could successfully demonstrate that the position and number of the bromine functionalities determines the 2D assembly structure through optimizing the intermolecular interactions.

---

* **The results presented in this chapter were published in:**

Tuan Anh Pham, Fei Song, Manh-Thuong Nguyen, Meike Stöhr, *Chem. Commun*., 2014, **50**, 14089-14092.

5.1 Introduction

Halogen bonding (X-bonding) is nowadays considered as a highly important tool in the field of crystal engineering and supramolecular chemistry [1-4]. In comparison to hydrogen bonding (H-bonding), X-bonding offers a tuneable interaction strength by properly choosing the halogen atoms as well as a higher directionality [5-8]. These unique properties make X-bonding an interesting alternative to the often employed and well-established H-bonding for achieving desired molecular architectures, which is considered to open up new pathways for the fabrication of molecular devices by the bottom-up approach. However, despite these exciting advantages, the use of X-bonding for controllably constructing on-surface supramolecular assemblies has only recently been recognised. For example, Lackinger *et al*. demonstrated the formation of two-dimensional (2D) supramolecular structures from tris-bromophenyl derivatives mediated by X-bonding at the solid–vacuum interface [9a], while Perepichka et al. reported the formation of 2D chiral structures from brominated tetrathienoanthracene derivatives at the solid-liquid interface [9b]. So far, however, only a few more studies investigated the influence of the chemical nature of the halogen substituents on the surface-supported self-assembly process [10–13]. It has been recognised that for the construction of such 2D structures, halogen substituents may play the determining role in the structural formation by balancing the delicate interplay between molecule-molecule and molecule-substrate interactions. Therefore, an in-depth understanding of the effects of halogen substituents on the resulting intermolecular interactions is of utmost importance for the usage of X-bonds for the construction of molecular devices.

Herein, we investigated the influence of the position and number of bromine substituents onto the formation of highly-ordered self-assembled structures as well as the resulting intermolecular interactions of pyrene derivatives on Au(111) under UHV conditions. For this purpose, two different pyrene derivatives, 1,3,6,8-tetrabromopyrene (Br_4Py) and 2,7-dibromopyrene (Br_2Py) were chosen, which possess four and two functional bromine groups, respectively, at different substituent positions. In order to minimize the effect of the substrate on the structural formation, we employed Au(111) as a substrate since it is generally considered less reactive than other noble metals [14].

5.2 Experimental results

5.2.1 Self-assembly of Br_4Py on Au(111)

Fig. 5.1 shows the chemical structure and the corresponding calculated electrostatic potential distribution of these molecules. Due to an anisotropic charge distribution around the halogen atom in a halogen-carbon bond, the bromine substituents in these molecules can act as both electrophiles and nucleophiles, allowing two different binding motifs at the same time [1, 5, 8, 15].

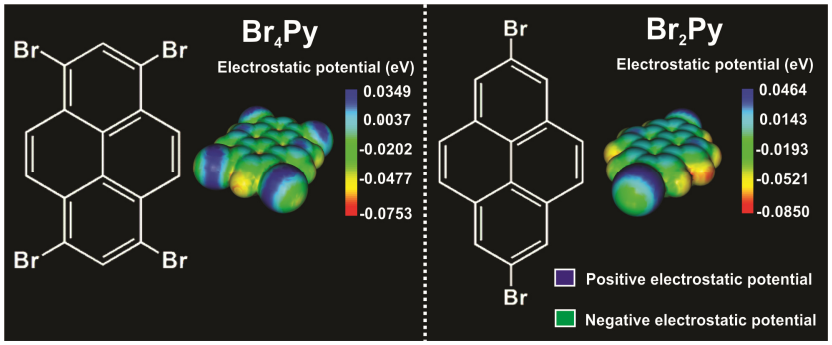

Figure 5.1: Chemical structure and corresponding electrostatic potential distributions of 1,3,6,8-tetrabromopyrene (Br_4Py) (left) and 2,7-dibromopyrene (Br_2Py) (right), respectively, showing the positive potential in blue and the negative potential in green/yellow at isodensity surfaces.

Upon deposition of Br_4Py on Au(111) held at room temperature, well-ordered 2D patterns were observed by STM under UHV conditions. Close to monolayer coverage, two different molecular arrangements coexist: a parallel arrangement (Fig. 5.2a, top and Fig. 5.2b) and a square arrangement (Fig. 5.2a, bottom and Fig. 5.2d), labelled phase I and II in the following, respectively. It should be noted that also at room temperature and for submonolayer coverage, Br_4Py forms islands exhibiting phase I. Phase I was found to be the dominant phase (occurrence of around 90%). In overview STM images for Br_4Py self-assembled into the phase I, the characteristic herringbone reconstruction of Au(111) is visible through the molecular adlayer (Fig. 5.3). This shows that the Au reconstruction is neither modified nor lifted upon adsorption of the molecules, indicating a weak molecule–substrate interaction. One axis of the molecular unit cell is rotated by approximately (7±1)° with respect to the principal Au direction. Interestingly, the molecules aligned in this unit cell direction undergo a small lateral shift with respect to each other at the positions at or close to the

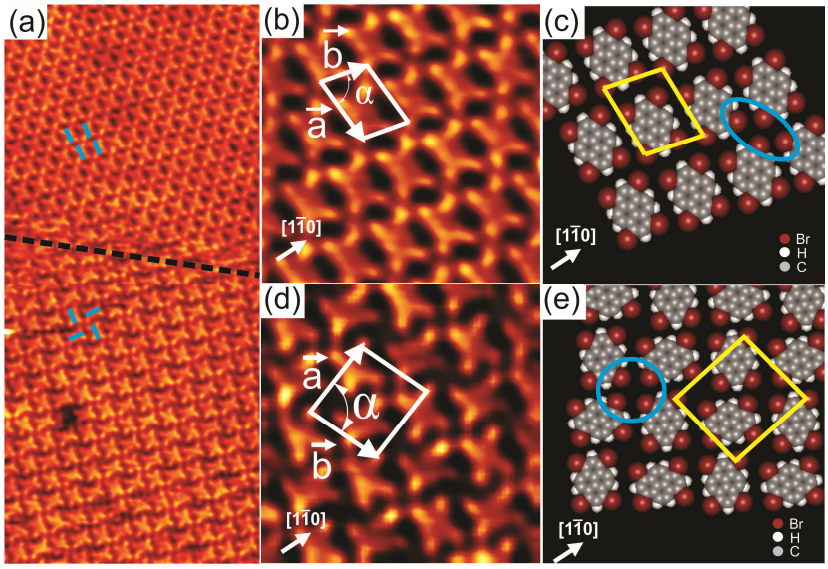

Figure 5.2: (a) Overview STM image (30×14 nm^2) for 1 ML Br_4Py on Au(111), showing the co-existence of two different molecular arrangements, labelled phase I (top) and phase II (bottom). (b, c) and (d, e) Close-up STM images (5×5 nm^2) and corresponding proposed molecular models for phase I and II, respectively. The STM images were taken at room temperature with U = -1.2 V, I = 60 pA.

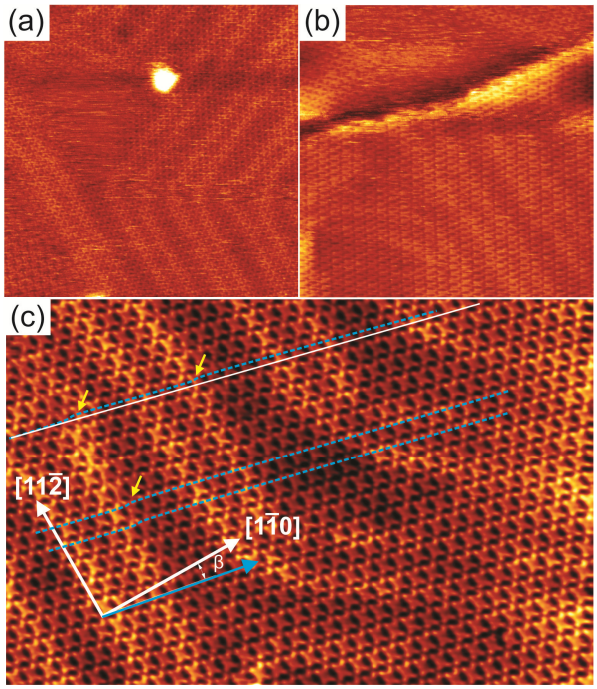

Figure 5.3: (a) Overview STM image (40×40 nm^2) showing that the herringbone reconstruction is intact under the molecular overlayer. (b) STM image (28×28 nm^2) showing the ordering of the molecules in the vicinity of a step edge. (c) STM image (20×30 nm^2) for 1 ML Br_4Py on Au(111). The principal substrate and molecular adsorption directions are denoted by white and blue arrows, respectively. β is the angle enclosed by the molecular adsorption direction and the [1$\bar{1}$0] substrate direction. The blue dotted lines act as a guide to the eye to indicate the slight shift of the molecular rows with respect to the straight white line. The STM images were taken at room temperature with U = -1.2 V, I = 80 pA.

soliton walls of the herringbone reconstruction [20]. The co-existence of three rotational domains having an angle of 120° to each other was observed, reflecting the threefold symmetry of the underlying substrate (Fig. 5.4). The molecular orientation in each of these domains is the same with respect to the underlying substrate. Taking these findings together, it turns out that the substrate has a weak but not negligible influence on the self-assembly process. Because the molecular lattice direction does not run parallel to a principal Au direction, it is expected that for each of the rotational domains, a mirror domain exists. Indeed, in STM images we observed rotational and mirror domains at the same time. Fig. 5.5 shows the existence of domains A_m and B_m, which are the mirror counterparts of domain A and B, respectively. The unit cell directions of "normal" and mirror domains enclose an angle of ± (7±1)º with a principal Au direction which is the mirror plane direction. In the high-resolution STM image in Fig. 5.2b, each Br_4Py molecule in phase I can be clearly discerned. Each molecule exhibits four bright protrusions corresponding to the four bromine substituents which is in good agreement with its chemical structure (Fig. 5.1). To precisely determine the unit cell parameters, also with respect to the underlying Au(111) substrate, low energy electron diffraction (LEED) measurements were performed (Fig. 5.6). An incommensurate superstructure was found for the molecules arranged into phase I. The unit cell contains one molecule and its lattice dimensions are found to be 11.7×8.8 Å^2 with an internal angle of 78°. It should be noted, that in LEED we did not obtain any spots arising from phase II. This further supports the fact that phase I, indeed, is the dominant phase upon adsorption of Br_4Py on Au(111) at monolayer coverage. Fig. 5.2c shows the proposed molecular model for phase I. The molecules align parallel with respect to each other. Four Br substituents of four neighbouring molecules point toward each other to form a fourfold node (marked by a blue ellipse in Fig. 5.2c). Each molecule connects to four such fourfold nodes. Because of the non-spherical charge distribution, each Br substituent can attractively interact with a negative charged Br or a positively charged H atom of adjacent molecules, forming so- called triangular binding motifs consisting of Br-Br and Br-H bonds, which are responsible for the network formation [9b]. In Fig. 5.2d individual Br_4Py molecules arranged into phase II are visible. The unit cell contains two molecules and

its dimensions are found to be a = (15.6 ± 0.2) Å, b = (14.4 ± 0.2) Å and α = (87 ± 1)º, as determined from STM measurements. The packing density of this phase is ~ 0.9 molecules nm^{-2}, whereas that of phase I is higher, ~ 1 molecule nm^{-2}. Within this phase, each molecule is surrounded by four neighbouring molecules rotated by 90° with respect to the central molecule. In the proposed molecular model (Fig. 5.2e), four molecules meet in a fourfold node formed by four Br substituents similar to what was observed for phase I. Only two of the four possible fourfold nodes (marked by a blue circle in Fig. 5.2e) have Br to Br and Br to H distances which are suitable for the establismnent of intermolecular interactions. Each molecule only participates in two such fourfold nodes what is in contrast to phase I. As observed for phase I, the molecular network is stabilised by triangular binding motifs based upon Br-Br and Br-H bonds. The basic unit of this molecular network is a chiral pinwheel-like tetramer resulting in organization chirality for the assembly. Both left- and right-handed homochiral domains were observed (Fig. 5.7).

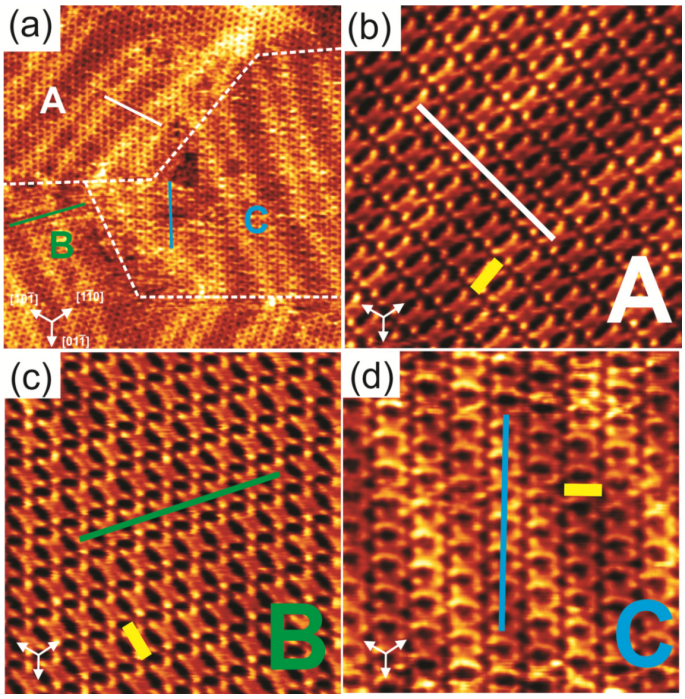

Figure 5.4: (a) Large scale STM image (38×38 nm^2) of 1ML Br_4Py on Au(111), showing the co-existence of three rotational domains, labeled A, B and C. The white dashed lines mark the domain boundaries. The solid white, green and blue lines in each domain indicate the molecular adsorption direction which is aligned along one of the principal Au directions. (b), (c) and (d) Close-up STM images (10×10 nm^2) of domains A, B and C, respectively. The short yellow line acts as a guide to the eye to indicate the molecular orientation for different domains with respect to the principal Au directions. The STM images were taken at room temperature with U = -1.2 V, I = 60 pA.

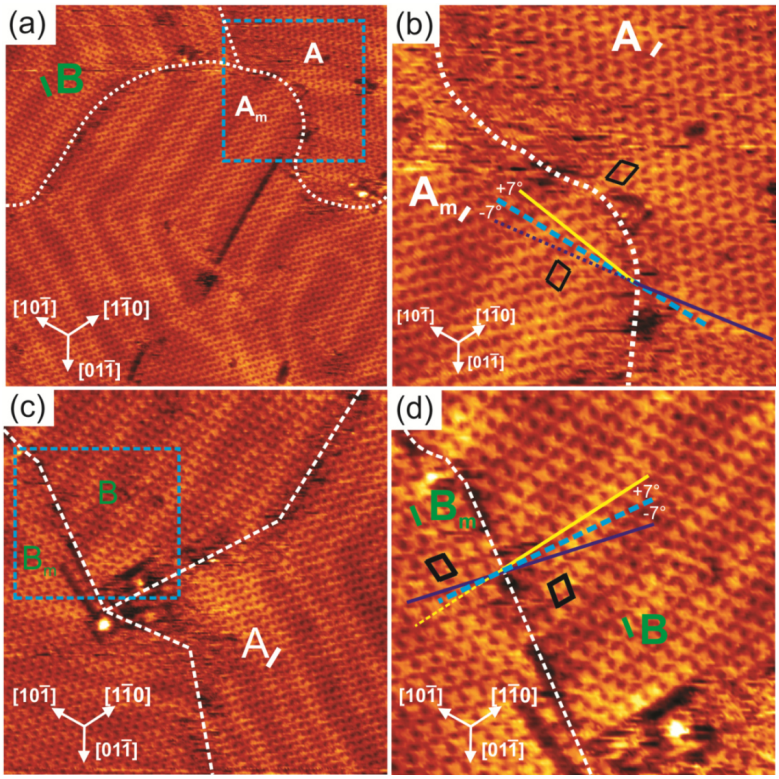

Figure 5.5: (a) and (c) Overview STM images (50×50 nm^2 and 35×35 nm^2, respectively) of 1 ML Br_4Py on Au(111), showing the co-existence of mirror domains. (b) and (d) Close-up STM images (20×20 nm^2 and 18×18 nm^2, respectively) of the areas marked by blue dotted squares in a) and c), respectively. The domain boundaries are marked by white dashed lines. The unit cells are marked by black rhomboids. The arrangement of the molecules within the unit cell is mirrored at the blue dotted line which is parallel to a principal Au direction. The set of three arrows indicates the principal directions of the substrate. The STM images were taken at room temperature with U = -1.47 V, I = 40 pA.

5.2.2 Self-assembly of Br_2Py on Au(111)

In order to examine the influence of the position and number of the Br substituents on the resulting intermolecular interactions responsible for the network formation, Br_2Py was deposited onto Au(111) held at room temperature. For monolayer coverage, the molecules arrange in a 2D brick-wall-like pattern which is labelled phase III (Fig. 5.8). Again, the characteristic herringbone reconstruction of Au(111) is observed through the molecular adlayer which is indicative of a weak molecule–substrate interaction. Each molecule exhibits two bright terminal protrusions corresponding to the two Br substituents (Fig. 5.8b). The unit cell contains one molecule and its lattice parameters are determined to be a = (11 ± 0.2) Å, b = (12.7 ± 0.2) Å and α = (52 ± 2)°. The packing density of this phase is found to be approximately 0.87 molecules nm^{-2} which

is lower than that of phase I and II. As can be seen in the proposed molecular model (Fig. 5.8c), the molecules align in parallel rows with their Br substituents in an antiparallel fashion, forming twofold nodes (marked by a blue circle in Fig. 5.8c). Importantly, this molecular arrangement does not form Br-Br bonds. Instead, the supramolecular network is stabilized by triangular binding motifs based on Br-H bonds enabled by the opposite charge regions of Br and H atoms within the twofold nodes. The absence of Br-Br bonds in phase III could be explained by taking thermodynamic considerations into account. It can be assumed that the interplay of

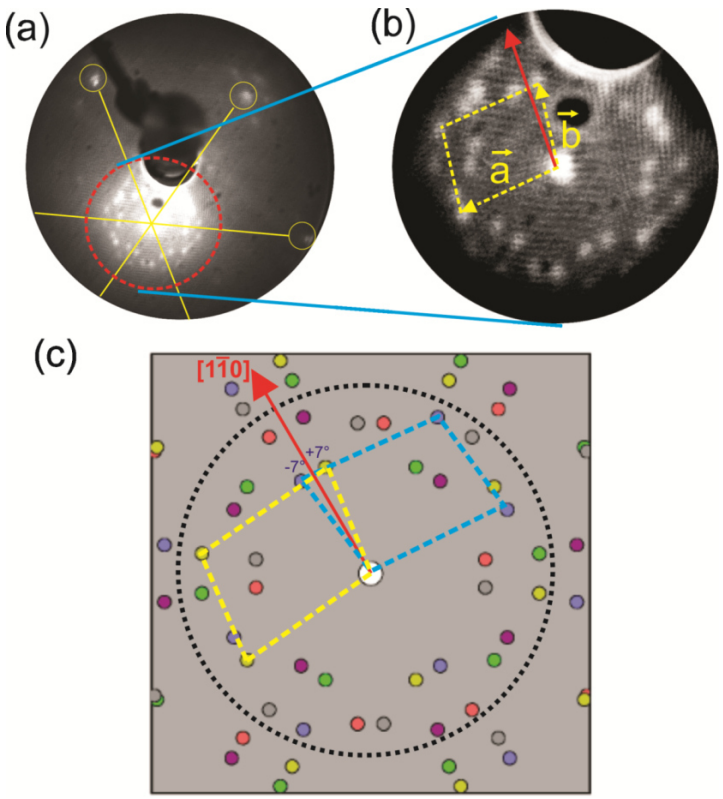

Figure 5.6: (a) LEED pattern for 1ML Br_4Py on Au(111) taken at a beam energy of 42 eV. The yellow lines act as a guide to the eye to mark the principal directions of the Au(111) substrate. The yellow circles mark the first order spots of the Au(111) substrate. (b) Zoom-in of the area marked by the red dashed circle in a). The unit cell of the molecular adlayer with corresponding vectors $\vec{a}$ and $\vec{b}$ is denoted by the yellow dashed rhomboid. The red arrow indicates one of the principal directions of the substrate. (c) Simulated LEED pattern. The black dashed circle marks the area where the diffraction spots are visible in b). The yellow and blue dashed rhomboids indicate the unit cells which are mirror images with respect to the principal Au direction. The angle enclosed between the principal Au direction and a unit cell vector amounts to 7° which is in excellent agreement with what is found from the STM analysis.

entropy and enthalpy plays an important role in the network formation [16, 17]. The decrease in entropy during the self-assembly must be compensated by a gain in enthalpy via the formation of favourable intermolecular interactions. Since Br_2Py has two terminal Br substituents, two adjacent molecules will preferably bind via Br-H bonds to maximize attractive interactions and to minimize repulsive Br-Br interactions. In this way a minimum in the Gibbs free energy is obtained corresponding to a stable state of the overall system.

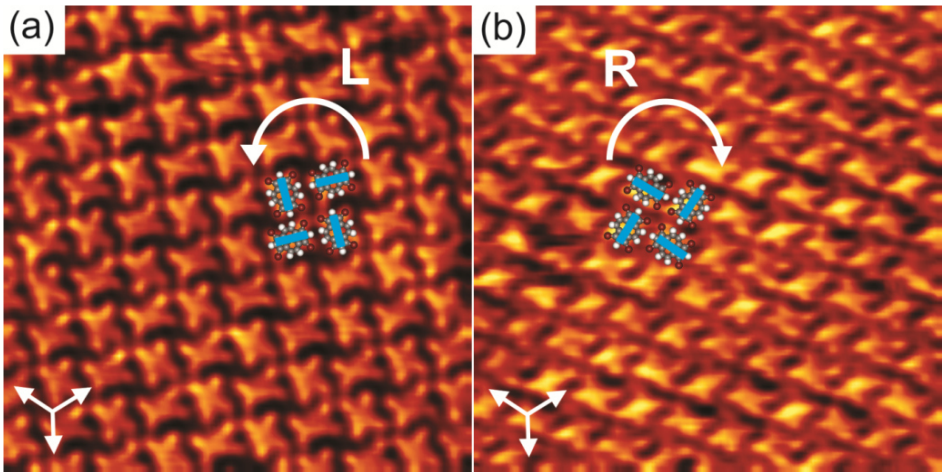

Figure 5.7: STM images (10×10 nm^2) of the self-assembled pinwheel structure of Br_4Py on Au(111) with (a) anticlockwise and (b) clockwise configuration. The solid blue lines on top of the molecules indicate the molecular orientations within each "pinwheel". The set of three arrows indicates the principal directions of the Au(111) substrate. The STM images were taken at room temperature with U = -1.4 V, I = 40 pA.

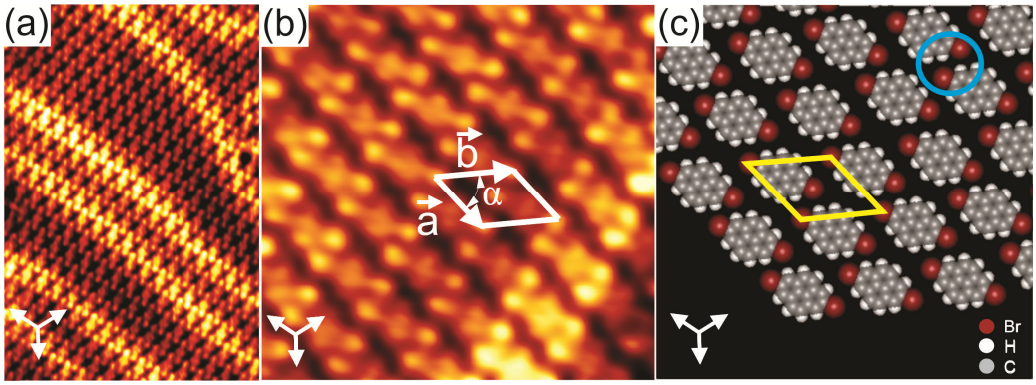

Figure 5.8: (a) Overview STM image (24×15 nm^2) for 1ML of Br_2Py on Au(111). (b) Close-up STM image (6.5×6.5 nm^2) and (c) corresponding proposed molecular model. The STM images were taken at 77 K with U = -1.8 V, I = 30 pA.

5.3 DFT calculations

In order to obtain a more detailed understanding of the intermolecular interactions, we carried out DFT calculations with van der Waals corrections included. The optimized intermolecular bonds are shown in Fig. 5.9 and the corresponding computed results are summarised in Fig. 5.10. It should be noted, that previously two different types of X-bonds were classified based on the bonding angle of the C–X groups [18]. The type-I X-bond is a repulsive interaction due the similar charge areas of the Br atoms pointing toward each other. This type occurs when $\theta_1 \approx \theta_2$ and their values fall in the range of 140^o to 180^o. Type-II X-bond is an attractive interaction between the positive and negative charge areas of the halogen atoms. This type occurs when the value of θ_1 falls in the range of 150^o to 180^o while that of θ_2 falls in the range of 90^o to 120^o [28-31]. The Br to Br distance for the formation of non-covalent bonds lies in the range of 3.4 to 3.9 Å [32]. For the formation of Br-H hydrogen bonds: if the Br to H distances are larger than 3.5 Å, this hydrogen bond is weak [33]. Then, it was not taken into account. In our case, the computed angles and distances between Br and H atoms fall in the range which is in good agreement with these values. These results confirmed the formation of Br-Br and Br-H bonds in triangular binding motifs which are responsible for the network formation. Combining this classification with our calculated results leads to an intuitive explanation for the occurring intermolecular interactions in the three networks. In both phases I and II, the molecular networks are mainly stabilized by $H_1 \cdots Br_4 \cdots Br_1$ and $H_3 \cdots Br_2 \cdots Br_3$ triangular binding motifs formed by Br-Br bonds (type-II) and Br-H bonds in each fourfold node. The main difference between these phases lies in the type-I repulsive interactions. The computed Br_1 to Br_3 distance shows that this repulsive interaction does not occur in phase II, but it may contribute to the sum of the driving forces for the network formation in phase I. For phase III, the molecular network is mainly driven by $H_1 \cdots Br_1 \cdots H_5$ and $H_3 \cdots Br_2 \cdots H_6$ triangular binding motifs formed by only Br-H bonds in each twofold node. The computed distances of $Br_1 \cdots H_4$, $Br_2 \cdots H_2$ and $Br_1 \cdots Br_2$ imply that the role of intermolecular interactions between parallel molecular rows running along the shorter unit cell axis can be neglected for the network formation [19].

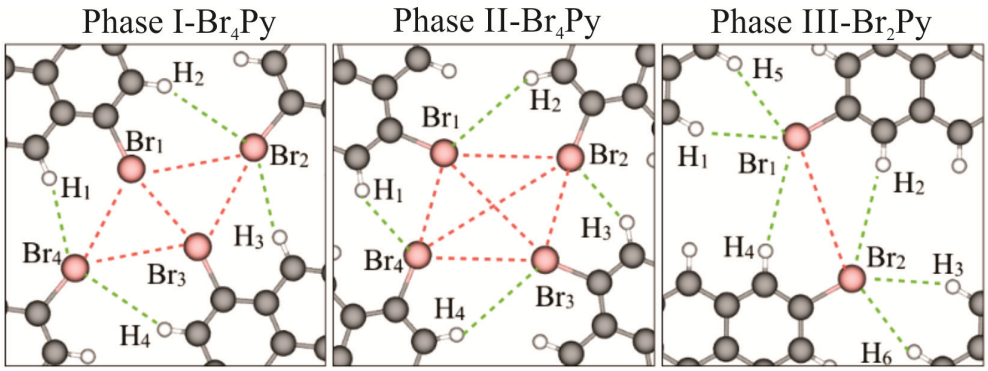

Figure 5.9: DFT optimized intermolecular interactions for phase I and II formed by Br_4Py and for phase III formed by Br_2Py molecules. The intermolecular Br-Br and Br-H bonds are marked by red and green dashed lines, respectively.

The calculated unit cells are entirely consistent with the experimental results (Fig. 5.11). The binding energies per molecule obtained from DFT calculations are 0.3 eV and 0.28 eV for phase I and phase II, respectively, whereas that of phase III is lower (0.21 eV). These results demonstrate that there are less intermolecular bonds per molecule in the case of phase III compared to that of phases I and II due to the differences in the position and number of Br substituents. However, the DFT calculations do not fully explain why for monolayer coverage almost exclusively phase I is observed. The reason for this could be substrate effects (presence of the herringbone reconstruction) which were not taken into account in our calculations.

5.4 Conclusions

In conclusion, we compared the self-assembly of pyrene derivatives on Au(111) under UHV conditions by combining STM experiments and DFT calculations. The Br_4Py molecules arrange into two different 2D patterns which are stabilized by X-bonds and Br-H bonds at the same time. On the other side, the 2D self-assembled pattern of Br_2Py is exclusively driven by Br-H bonds. These results successfully demonstrate that the positions and number of Br substituents determine the final supramolecular networks of pyrene derivatives on Au(111).

(a)

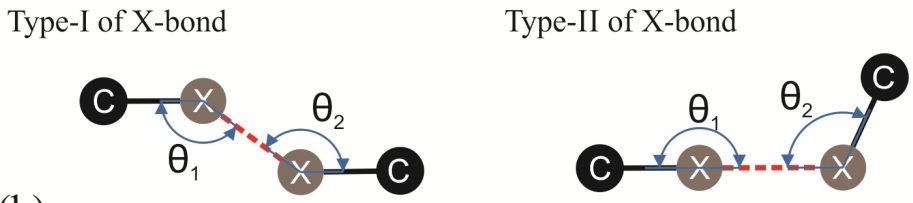

(b)

Phase I-Br_4Py

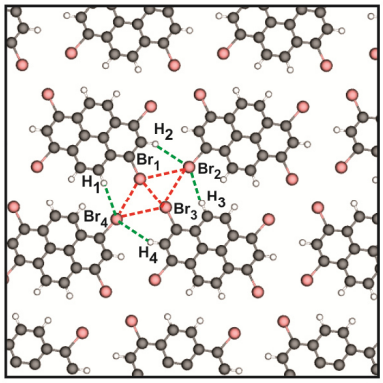

Distance/Å		Angle/°			
Br_1Br_2	4.07	CBr_1Br_2	106.3	CBr_2Br_1	139.6
Br_1Br_4	3.72	CBr_1Br_4	124.2	CBr_4Br_1	169.9
Br_3Br_4	4.07	CBr_3Br_4	106.3	CBr_4Br_3	139.6
Br_2Br_3	3.72	CBr_2Br_3	124.2	CBr_3Br_2	169.9
Br_1Br_3	3.34	CBr_1Br_3	165.6	CBr_3Br_1	165.6
Br_4H_1	3.04	CBr_4H_1	124.0	CH_1Br_4	172.8
Br_4H_4	3.55	CBr_4H_4	95.5	CH_4Br_4	152.7
Br_2H_3	3.04	CBr_2H_3	124.0	CH_3Br_2	172.8
Br_2H_2	3.55	CBr_2H_2	95.5	CH_2Br_2	152.7

Phase II-Br_4Py

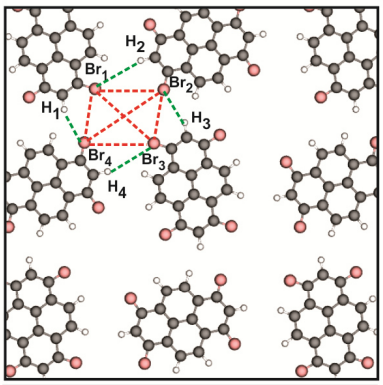

Distance/Å		Angle/°			
Br_1Br_2	4.00	CBr_1Br_2	161.0	CBr_2Br_1	110.1
Br_1Br_3	4.80	CBr_1Br_3	152.3	CBr_3Br_1	152.3
Br_1Br_4	3.56	CBr_1Br_4	97.2	CBr_4Br_1	171.6
Br_2Br_4	5.87	CBr_2Br_4	146.5	CBr_4Br_2	146.5
Br_1H_2	3.68	CBr_1H_2	117.0	CH_2Br_1	149.4
Br_2H_3	2.81	CBr_2H_3	118.1	CH_3Br_2	151.3

Phase III-Br_2Py

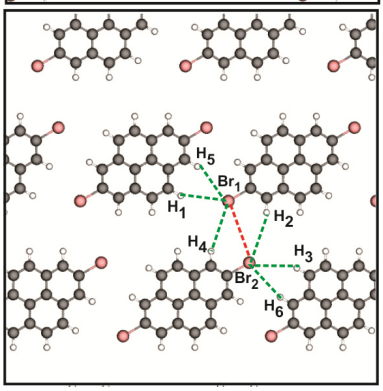

Distance/Å		Angle/°			
Br_1Br_2	4.95	CBr_1Br_2	97.8	CBr_2Br_1	97.8
Br_1H_1	3.31	CBr_1H_1	146.2	CH_1Br_1	154.4
Br_1H_4	3.85	CBr_1H_4	134.5	CH_4Br_1	166.2
Br_1H_5	3.13	CBr_1H_5	101.4	CH_5Br_1	161.2
Br_2H_3	3.31	CBr_2H_3	146.2	CH_3Br_2	154.4
Br_2H_2	3.85	CBr_2H_2	134.5	CH_2Br_2	166.2
Br_2H_6	3.13	CBr_2H_6	101.4	CH_6Br_2	161.2

Figure 5.10: (a) Illustration for two different types of X-bonds. (b-d) DFT optimized intermolecular interactions and summarized computed distances and angles for Br-Br and Br-H intermolecular bonds of Br_4Py and Br_2Py molecules.

(a)

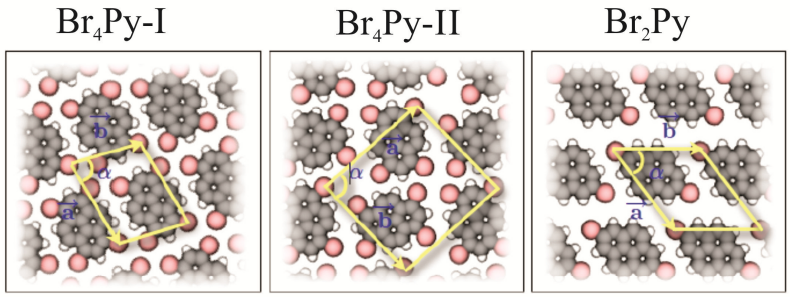

(b)

	Br_4Py-I	Br_4Py-II	Br_2Py
$\lvert\vec{a}_e\rvert$ (Å)	11.2	15.6	11
$\lvert\vec{b}_e\rvert$ (Å)	8.7	14.4	12.7
α_e(°)	73	87	52
$\lvert\vec{a}_0\rvert$ (Å)	11.7	15.4	10.8
$\lvert\vec{b}_0\rvert$ (Å)	9.1	14.3	12.5
α_0(°)	75	87	52
$\lvert\vec{a}_1\rvert$ (Å)	11.7		
$\lvert\vec{b}_1\rvert$ (Å)	8.8		
α_1(°)	78		
ΔE (eV)	0.3	0.28	0.21

Figure 5.11: (a) DFT optimized unit cell and (b) corresponding geometric and energetic properties for different molecular networks of Br_4Py and Br_2Py. Subscripts e, 1 and 0 in (b) imply the experimentally obtained values from STM, LEED and the computed values, respectively.

5.5 Experimental methods and computational details

5.5.1 Experimental methods

The STM experiments were carried out in two independent two-chamber ultra-high vacuum systems with a base pressure of 5×10^{-10} mbar. Both systems are equipped with facilities for surface preparation, i.e. Ar^+ ion sputtering and resistive sample heating. The first system houses a variable temperature STM (Oxford Instruments Omicron NanoScience) and a LEED apparatus (SPECS Surface Nano Analysis GmbH). The second system houses a low-temperature STM (Oxford Instruments Omicron NanoScience). The Au(111) single crystal was prepared by repeated cycles of sputtering with Ar^+ ions and annealing at approximately 400°C. Commercially available 1,3,6,8–tetrabromopyrene (Br_4Py) and 2,7–dibromopyrene (Br_2Py) were thoroughly degassed several hours before deposition onto Au(111). The molecules

were thermally evaporated from a glass crucible that was heated inside a home-built evaporator. The deposition rate was monitored using a quartz crystal microbalance in order to determine the molecular coverage. The substrate was held at room temperature during deposition. The STM images of Br_4Py/Br_2Py were taken in constant current mode using a platinum-iridium tip at room temperature/77K. The bias voltage is applied to the tip while the sample is grounded. Image processing was done with the free software WSxM [21].

LEED measurements were performed to determine the molecular unit cell for the close-packed assembly obtained after deposition of Br_4Py on Au(111) held at room temperature. The LEED pattern was taken for samples held at room temperature. The sample was slightly tilted with respect to normal incidence, allowing the observation the diffraction spots of first order which would be otherwise hidden by the electron gun. The LEED pattern was taken at an energy of 42 eV for the incident electron beam. The software LEEDpat2.1 was used to simulate the experimentally obtained LEED pattern [22].

5.5.2 Computational details

Plane-wave density functional theory calculations were carried out using the Quantum ESPRESSO package [23], within the framework of the PBE [24] density functional corrected with semi-empirical dispersion potentials [25] as the van der Waals interactions play a key role in the stability of non-covalently bonded molecules [26]. Additionally, the projector augmented-wave method was employed [27]. We used a kinetic energy cutoff of 40 Ry.

We optimized the geometry of single Br_4Py and Br_2Py in a 22×22×20 $Å^3$ unit cell. Concerning molecular networks, the starting unit cell parameters were chosen from experiments, details are given below. The unit cells were then optimized with the force convergence threshold of 10^{-4} eV/Å. A 2×3×1, 2×2×1, and 2 × 2 × 1 k−point grid was used to sample the Brillouin zone in the self-consistent calculations for phase I, phase II of Br_4Py, and Br_2Py supramolecular nanostructures, respectively. In the geometry optimization processes, the molecules were kept co-planar as they are supposed to be adsorbed on Au(111) in a flat-lying fashion with the same molecule-

surface separation. Binding energy per molecule in the molecular networks was calculated as

$$\Delta E = \frac{E_{network} - nE_{single}}{n}$$

where E_{network} is the energy of a unit cell in the network, n (n = 1, 2) is the number of molecules making up the unit cell, and E_{single} is the energy of a single molecule.

The electrostatic potential was calculated as the sum of the potential generated by ions and the Hartree potential.

References

[1] P. Metrangolo, F. Meyer, T. Pilati, G. Resnati and G. Terraneo, *Angew. Chem. Int. Ed.*, 2008, **47**, 6114.

[2] L. Meazza, J. A. Foster, K. Fucke, P. Metrangolo, G. Resnati and J. W. Steed, *Nat. Chem.*, 2013, **5**, 42.

[3] R. W. Troff, T. Makela, F. Topic, A. Valkonen, K. Raatikainen and K. Rissannen, *Eur. J. Org. Chem.,* 2013, **9**, 1617.

[4] H. M. Titi, R. Patra and I. Goldberg, *Chem. Eur. J.*, 2013, **19**, 14941.

[5] P. Politzer, J. S. Murray and T. Clark, *Phys. Chem. Chem. Phys.,* 2010, **12**, 7748.

[6] C. B. Aakeroy, M. Baldrighi, J. Desper, P. Metrangolo and G. Resnati, *Chem. Eur. J.,* 2013, **19**, 16240.

[7] A. Priimagi, G. Cavallo, P. Metrangolo and G. Resnati, *Acc. Chem. Res.,* 2013, **46**, 2686.

[8] S. M. Huber, J.D. Scanlon, E. J. Izal, J. M. Ugalde and I. Infante, *Phys. Chem. Chem. Phys*., 2013, **15**, 10350.

[9] a) H. Walch, R. Gutzler, T. Sirtl, G. Eder and M. Lackinger, *J. Phys. Chem. C*, 2010, **114**, 12604; b) R. Gutzler, O. Ivasenko, C. Fu, J. L. Brusso, F. Rosei and D. F. Perepichka, *Chem. Commun*., 2011, **47**, 9455.

[10] a) K. H. Chung, J. Park, K. Y. Kim, J. K. Yoon, H. Kim, S. Han and S. J. Kahng, *Chem.Commun*., 2011, **47**, 11492.; b) K. H. Chung, H. Kim, W. J. Jang, J. K. Yoon, S. J. Kahng, J. Lee and S. Han, *J. Phys. Chem. C*, 2013, **117**, 302.

[11] a) J. K. Yoon, W. J. Son, H. Kim, K. H. Chung, S. Han and S. J. Kahng, *Nanotechnology*, 2011, **22**, 275705.; b) Y. Makoudi, B. Baris, J. Jaeannoutot, F. Palmin, B. Grandidier and F. Cherioux, *Chem. Phys. Chem.*, 2013, **14**, 900.

[12] B. Cui, H.J. Yan, D. Wang and L.J. Wan, *J. Electroanal. Chem.,* 2013, **668**, 237.

[13] N. M. Jenny, H. Wang, M. Neuburger, H. Fuchs, L. Chi and M. Mayor, *Eur. J. Org. Chem*., 2012, 2738.

[14] F. S. Tautz, *Prog. Surf. Sci*. 2007, **82**, 479.

[15] K. E. Riley and P. Hobza, *Phys. Chem. Chem. Phys*., 2013, **15**, 17742.

[16] G. M. Whitesides, J. P. Mathias, C.T. Seto, *Science*, 1991, **254**, 1312.

[17] N. Wintjes, J. Hornung, J. L. Checa, T. Voigt, T. Samuely, C. Thilgen, M. Stöhr, F. Diederich, T. A. Jung, *Chem. Eur, J*., 2008, **14**, 5794.

[18] T. T. T. Bui, S. Dahaoui, C. Lecomte, G. R Desiraju and E. Espinosa, *Angew. Chem. Int. Ed*., 2009, **48**, 3838.

[19] F. Lieberman, R. J. Davey and D. M. T. Newsham, *Chem. Matter*., 2000, **12**, 490.

[20] Chizhov, G. Scoles, A. Kahn, *Langmuir*, 2000*,* **16***,* 4358.

[21] I. Horcas, R. Fernández, J. M. Gómez-Rodríguez, J. Colchero, J. Gómez-Herrero, A.M. Baro. *Rev. Sci. Intrum*., 2007, **78**, 013705.

[22] http://www.fhi-berlin.mpg.de/KHsoftware/LEEDpat/.

[23] P. Giannozzi, S. Baroni, N. Bonini, M. Calandra, R. Car, C. Cavazzoni, D. Ceresoli, G. L. Chiarotti, M. Cococcioni, I. Dabo, A. Dal Corso, S. de Gironcoli, S. Fabris, G. Fratesi, R. Gebauer, U. Gerstmann, C. Gougoussis, A. Kokalj, M. Lazzeri, L. Martin-Samos, N. Marzari, F. Mauri, R. Maz- zarello, S. Paolini, A. Pasquarello, L. Paulatto, C. Sbraccia, S. Scandolo, G. Sclauzero, A. P. Seitsonen, A. Smogunov, P. Umari, and R. M. Wentzcovitch, *J. Phys.:Condens. Matter*. 2009, **21**, 395502.

[24] J. P. Perdew, K. Burke, and M. Ernzerhof, *Phys. Rev. Lett*., 1996, **77**, 3865.

[25] S. Grimme, *J. Comp. Chem*., 2006, **27**, 1787.

[26] K. E. Riley and P. Hobza, *Phys. Chem. Chem. Phys*., 2013, **15**, 17742.

[27] G. Kresse and D. Joubert, *Phys. Rev. B*., 1999, **59**, 1758.

[28] B. K. Saha, R. K. R. Jetti, S. Reddy, S. Aitipamula and A. Nangia, *Cryst. Growth Des*., 2005, **5**, 887.

[29] N. Ramasubbu, R. Parthasarathy and P. Murray-Rust, *J. Am. Chem. Soc*., 1986, **108**, 4308.

[30] F. Silly, *J. Phys. Chem. C*, 2013, **117**, 20244.

[31] J. K. Yoon, W.J. Son, K. H. Chung, H. Kim, S. Han and S. J. Kahng, *J. Phys. Chem. C*, 2011, **115**, 2297.

[32] R. Gutzler, O. Ivasenko, C. Fu, J. L. Brusso, F. Roise and D. F. Perepichka, *Chem. Commun*., 2011, **47**, 9455.

[33] P. M. Pihko. *Hydrogen Bonding in Organic Synthesis*. Willey-VCH Verlag GmbH & Co. KGaA, Weinheim, 2009.